JOURNAL OF AIRCRAFT
Vol. 37, No. 2, March–April 2000

Numerical Simulation of Rotor Flow in Hover

Guowei Yang* and Lixian Zhuang†
University of Science and Technology of China, Hefei, 230026 Anhui, People's Republic of China

Aerodynamic loads on a multibladed helicopter rotor in hovering flight are calculated by solving the unsteady three-dimensional Reynolds-averaged Navier–Stokes equations. It is well known that, because of the numerical diffusion, the rotor-wake effects cannot be properly simulated by a Navier–Stokes calculation with a moderate grid number, which leads to the calculated suction pressures higher than the experimental values. The rotor-wake effects are then accounted for by the correction of local geometric angle of attack according to a free-wake modeling in addition to an empirical modification for the tip flow effects. The validity and efficiency of the present method have been verified by the comparisons between numerical results and experimental data.

Introduction

TO calculate the aerodynamic performance of a helicopter in hovering flight is a problem of great practical importance as well as the theoretical complexity. Theoretically, a solution of the full Navier–Stokes equations with appropriate turbulence modeling and body-conforming grid is sufficient for a good description of all of the physics involved. But unlike the flowfield around a fixed wing, the trailing vortex wake of a rotary wing rotates with the rotor and is shed to a far distance below the rotor plane by its self-induced velocity. The helical vortex sheet interacts strongly with the lifting surfaces, but this process is hard to be simulated unless using a quite clustered grid, which generally requires very large computational resource. Srinivasan et al.,[1] using about one million grid number to solve the thin-layer Navier–Stokes equations, calculated the whole flowfield including the induced effects of the wake and the interaction of tip vortices with successive blades, but they also found their captured vortex structure was overdiffused because of the coarse grid used.

The current methods for calculating rotor performance usually solve the potential, Euler, or Navier–Stokes equations coupled with an external free- or rigid-wake model based on the lift line or lift surface theory.[2–6] But it is clear that these governing equations are hard to match with the linear trailing wake modeling in a physically consistent manner. Further, those approaches also require fairly large computer resource from solving two coupled models simultaneously.

Agarwal and Deese[7] calculated the aerodynamic loads by solving the thin-layer Navier–Stokes equations, and the rotor-wake effects were modeled with a correction applied to the geometric angle of attack along the blades. This correction was obtained by computing the local induced downwash by the rotor wake with a free-wake analysis program. In fact, this method just established a weaker link between the rotor and its wake and avoided the complex boundary handling and the solution of coupled equations. Therefore, the grid number used is not huge, and the accuracy of calculated results is satisfactory.

In the present paper we essentially borrowed the approach from Ref. 7, but extended it to the solution of a complete Navier–Stokes equation, rather than a thin-layer one. In addition, an improved method is suggested to obtain a proper correction of the local angle of attack of the blades. This is constructed by the comparison between the results with and without rotor wake modeling, in addition to a heuristic consideration of the coupling rotor-wake and three-dimensional blade-tip effects that is expressed by a semi-empirical formula. The results calculated using the present computational method are compared with the available experimental data and are proved to be in good agreement with them, which demonstrated the reliability and efficiency of the present method.

Received 23 July 1998; revision received 5 April 1999; accepted for publication 30 August 1999.

*Associate Professor, Department of Mechanics and Mechanical Engineering.
†Professor, Department of Mechanics and Mechanical Engineering.

Computational Grid

Body-conforming, single-block, three-dimensional computational grids were constructed for the rectangular rotor blades[8] by stacking and bending two-dimensional H grids, which were generated by solving an elliptic equation.[9] For hover cases only the flow about one blade needs to be simulated because the flow is periodic from blade to blade. A cylindrical H-grid topology was chosen. Unlike the grid of fixed wing, here the two-dimensional H grid in each spanwise position takes the local effective angle of attack into account. For a single case the grid system is generated once and for all, but for different calculated conditions, say at different Mach numbers, the new grid must be regenerated in a similar way. Figure 1 illustrates the typical grid structure of the rotor. Figure 1a shows the cylindrical nature of the grid in the plane of the rotor, and Fig. 1b shows a typical two-dimensional H grid in a spanwise station. The coordinate system is chosen such that x is in the chordwise direction, y is in the spanwise direction, and z is in the normal direction.

The grids used here have 100 grid points in the wraparound direction with 30 points on the body, 35 points in the spanwise direction with 25 points on the blade surface, and 45 points in the normal direction with 25 points below the rotor grid plane. The grid was clustered near the leading and trailing edges and near the tip region to resolve the tip vortex. It was also clustered in the normal direction to resolve the boundary layer near the blade surface. One can see that the total grid number in this method is not so large, but still the calculated results are satisfactory. This is just the key point that we prefer to recommend the present method.

Computational Method

The governing equations are the three-dimensional unsteady compressible Navier–Stokes equations in an instantaneous inertial frame of reference. Written in a conservative form with a generalized body-fitted curvilinear coordinate, it is

$$\partial_\tau Q + \partial_\xi E + \partial_\eta F + \partial_\zeta G = \partial_\xi E_v + \partial_\eta F_v + \partial_\zeta G_v \qquad (1)$$

where Q are the conserved quantities; E, F, and G are the inviscid flux vectors; and E_v, F_v, and G_v are the viscous flux vectors. The generalized coordinates $\tau = t$, $\xi = \xi(x, y, z, t)$, $\eta = \eta(x, y, z, t)$, and $\zeta = \zeta(x, y, z, t)$ are attached to the blade.

For an instantaneous inertial frame of reference fitting to the rotating wing, the orientations of the x axis and y axis must be changed with time but still be fixed to the undisturbed fluid at infinity. Then the grid system can always be attached to the blades and generated once and for all in a single case. The time derivative term in Eq. (1), however, should be carefully calculated in a proper way. We prefer

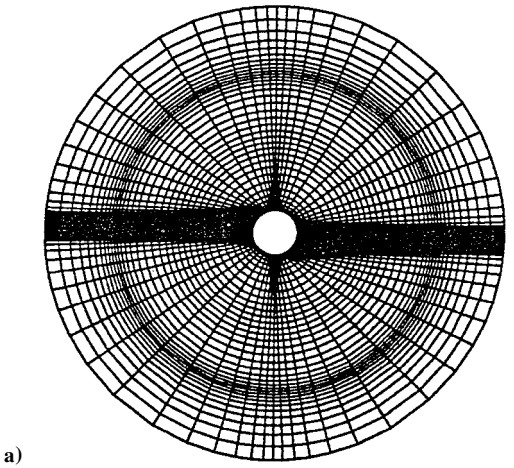

a)

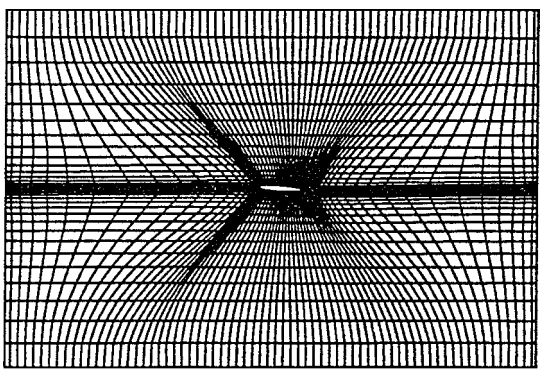

b)

Fig. 1 H-type grid for the two-bladed rotor in hover.

to use this frame of reference because it is easier to handle the far-field boundary conditions in this frame than in a noninertial rotating frame and keep the mesh to be blade fixed.

The inviscid and viscous fluxes are evaluated using a second-order central difference with a fourth-order artificial viscosity.[10] The implicit operator for time stepping is the lower upper symmetric Gauss-Seidel (LU-SGS) scheme.[11] This operator takes the form

$$LD^{-1}U\Delta q^n = -\Delta\tau R(q^n) \tag{2}$$

where D, L, and U are diagonal, lower, and upper tridiagonal matrices, respectively, $\Delta q^n = Q^{n+1} - Q^n$, and $\Delta\tau$ is the time step. The term $R(q)$ consists of the spatial difference of the inviscid and viscous flux vectors at time level n.

$$R(q^n) = \partial_\xi E + \partial_\eta F + \partial_\zeta G - (\partial_\xi E_v + \partial_\eta F_v + \partial_\zeta G_v) \tag{3}$$

To reduce the implicit factorization error, inner relaxation iterations at each time step are applied as follows: using the solution at time level n, setting the initial condition to $Q^{n+1,0} = Q^n$ and applying LU-SGS to solve the following equation in each inner iteration:

$$(LD^{-1}U)^{n+1,m}\Delta q^{n+1,m} = -\Delta\tau[(Q^{n+1,m} - Q^n)/\Delta\tau + R(q^{n+1,m})] \tag{4}$$

where $\Delta q^{n+1,m} = Q^{n+1,m+1} - Q^{n+1,m}$. The variable n refers to the time level $t = t_n$, and m refers to the iteration level. Three inner iterations were used for the unsteady cases in this work. Completing the inner iterations, the solution at the next time level is set to be

$$Q^{n+1} = Q^{n+1,m_{\max}}$$

For turbulent viscous flows the nondimensional viscosity coefficient in viscous fluxes is computed as the sum of $\mu_l + \mu_t$, where μ_l, the laminar viscosity, is estimated using Sutherland's law and μ_t, the turbulent viscosity, is evaluated using the Baldwin–Lomax algebraic eddy viscosity model.[12]

Boundary Conditions

In the calculation procedure the rotor blade is started from rest in a quiescent fluid, and the evolution of the flowfield is monitored as the blade moves azimuthally.

All of the boundary conditions are applied explicitly. At the wall a no-slip boundary condition is used for the viscous calculations. To ensure continuity across the wake cut and also outboard of the blade tip, where the grid collapses to a singular plane because of H-grid topology, the flow quantities are determined by averaging the flow variables from both sides of the singular plane.

To capture the information in the wake region of the blade, a periodical condition is used in the azimuthal direction that swaps the flow information, after interpolation, at the front and back boundaries of the cylindrical grid. The radial inboard and far-field boundaries as well as the top boundary are handled by one-dimensional characteristic boundary conditions.

On the outflow boundary below the rotor plane, the specification of the flow velocity is dictated from the momentum theory. At the flow exit of a circular hole whose area is half of the rotor disk, the outflow velocity is as much as twice the momentum theory value averaged on the plane of the rotor. In practical calculation the average velocity is calculated in a grid plane just on the edge of the blade viscous region. Other flow variables are extrapolated from within.

Loading Calculation Without Angle Correction

The test cases considered here correspond to the experimental hover conditions of Caradonna and Tung.[8] The experimental model consists of a two-bladed rigid rotor with rectangular planform blades and no twist or taper. The blades adopt NACA 0012 airfoil sections with an aspect ratio of 6. The inboard plane near the axis of rotation was located at a radial station equal to one chord.

Theoretically, the numerical solution to the full Navier–Stokes equations without rotor wake modeling seems to be capable of simulating all physics of the flow. The first calculation is then performed for a nonlifting case with a tip Mach number of $M_t = 0.52$, collective pitch $\theta_c = 0$ deg, and the Reynolds number based on the blade-tip speed and chord $Re = 2 \times 10^6$. Figure 2 shows the surface-pressure distribution at different spanwise locations. Sure enough, the agreement between the calculation and experiment is excellent.

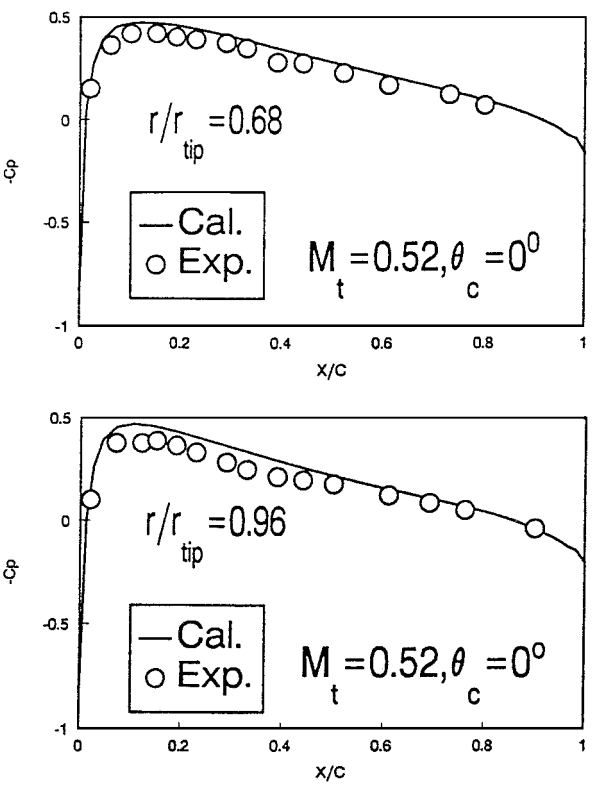

Fig. 2 Surface pressure for nonlifting case.

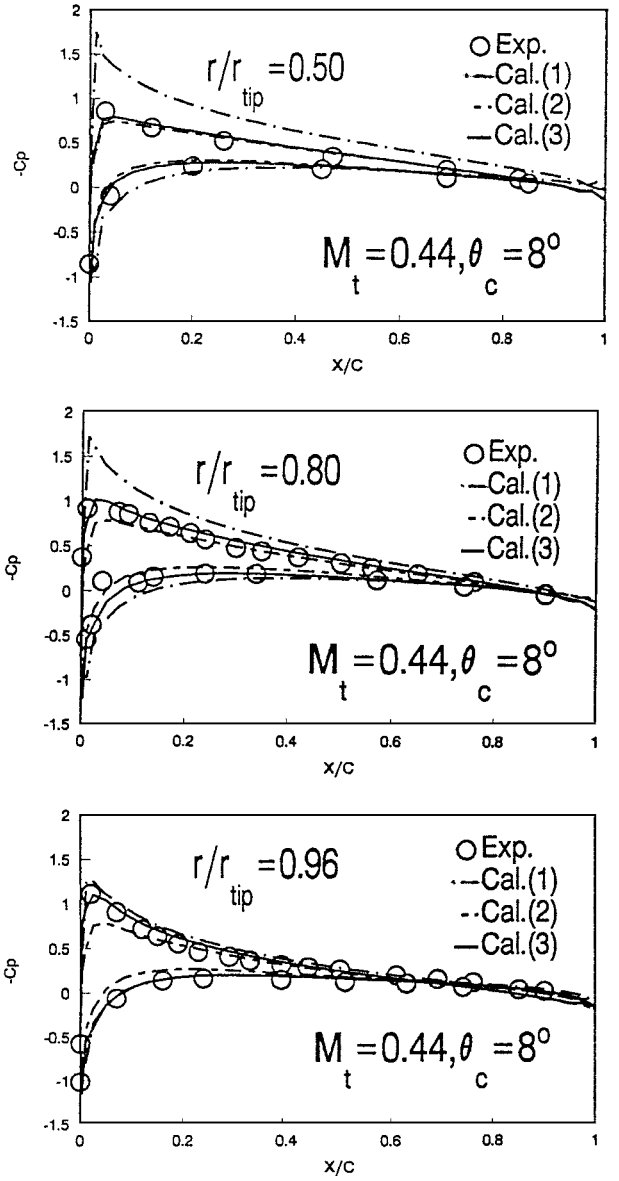

Fig. 3 Surface pressure coefficients.

Then we calculate the lifting case for $M_t = 0.44$, $Re = 2 \times 10^6$, $\theta_c = 8$ deg. Figure 3 shows the surface pressure distribution at different spanwise stations, and the calculated result is shown as Cal.(1) in this figure. The pressure distribution shows much stronger suction peaks at the leading edge than those observed experimentally, but near the rotor-tip region the loading matches well with the experiment data.

This situation comes from the following fact. In the nonlifting case the vorticity is limited to a thin layer at the vicinity of rotor plane so that the rotor wake can be correctly simulated and the calculated pressure is in good agreement with the experimental data. On the other hand, for the lifting case the helical trailing vortex moves along its axial direction up to far below the rotor plane, and this trailing vortex has strong effects on the rotor loading. Because of the numerical dissipation of coarse grid, the Navier–Stokes calculation cannot simulate such a helical trailing vortex correctly. A cheap way to solve this problem is to add an external rotor vortex model to the Navier–Stokes calculation to reflect the effective angle of attack of the rotor blades. Another fact, however, is that near the rotor tip the calculated loading without vortex modeling still matches well with the experiment data. Roberts and Murman[3] pointed out that the loading at the blade-tip region is dominated by three-dimensional tip effects and is relatively insensitive to the rotor trailing vortex. In view of this, we suggested a further modification to improve the simple trailing vortex correction by a formula mentioned next.

Wake Modeling

In Ref. 13, the authors developed a free-wake analysis for simulating the propeller slipstream flowfield based on the lift line theory. Here, the code is extended to the rotor flow calculation. The main difference is that the propeller slipstream moves along its axial direction because of the effect of freestream axial flow, but the motion of rotor wake is a self-induced one. Now the free-wake modeling is described as follows.

The initial shape of the helical vortex wake of the rotating blades is given by

$$x_i = r_i \sin(\theta + \theta_p), \qquad y_i = r_i \cos(\theta + \theta_p), \qquad z_i = (v_{zi}/\omega r_{tip})\theta \tag{5}$$

where θ is angle of rotor rotation, r_i is the horizontal radius of the helical vortex line, ω is the angle velocity of the rotor, r_{tip} is the radius of the rotor tip, v_{zi} represents the axial induced velocity, $\theta_p = 2\pi(k-1)/p$, and p is the rotor blade number. The multibladed interference is considered in the calculation when k is taken from 1 to p. The initial helical vortex lines represented by Eq. (5) are divided into a near-vortex wake and a far-vortex wake region; the near-wake region is composed of free-line vortex chains, and the trailing-vortex contraction effect is considered only in this region. The far-wake region consists of the equal-pitch and equal-diameter helical vortex lines determined by the last point parameter of the near-wake region. In the paper the near-wake region extended to the $\theta = 3600$ deg rotational azimuth downstream of the blade. A relaxation iteration scheme of the free near wake was constructed. Through this iterative calculation a contraction rotor wake can be obtained. The detail can be seen in Ref. 13.

For $M_t = 0.44$, $Re = 2 \times 10^6$, $\theta_c = 8$ deg, the rotor-wake contraction calculated by the free-wake modeling is shown in Fig. 4. The compressibility effect is considered through the Prandtl–Glauert rule. It is clear that the wake contraction mainly occurs in the vicinity below the blade and the contraction value is about 10%, which can be regarded as qualitatively reasonable.

Loading Calculation with Angle Correction

After the contraction wake shape is determined, the axial-induced velocity along the rotor blade can be calculated, and the effective

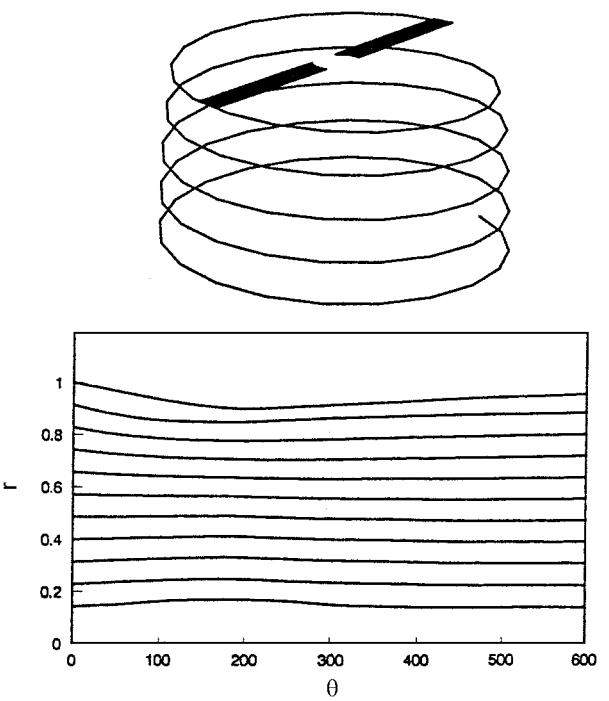

Fig. 4 Rotor-tip wake and its contraction radius corresponding to the rotational azimuth.

angle of attack along the spanwise direction is then calculated by the following formula:

$$\alpha_{\text{eff}}(r) = \theta_c - \tan^{-1}[v_z(r)/\omega r] \tag{6}$$

where $v_z(r)$ is the axial-induced velocity at the rotor spanwise position r. The distribution of effective angle of attack along the blade is given in Fig. 5, corresponding the case Cal.(2). The effective angles are smaller than the collective pitch angle $\theta_c = 8$ deg, particularly on the inboard part of the blade.

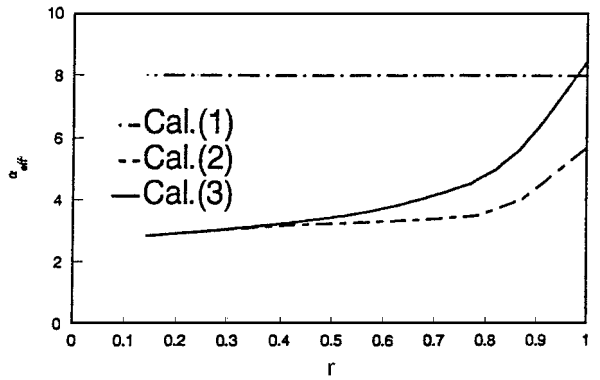

Fig. 5 Distribution of effective angle of attack.

Using the local effective angle of attack, we recalculated the rotor loading with the Navier–Stokes solver. The calculated pressure distributions are shown in Fig. 3, corresponding the Cal.(2). The calculated result is much better than that of Cal.(1). The pressure is in good agreement with the experimental data in the middle spanwise station $y/R = 0.5$, but does not agree quite well with the experimental results at the tip region. As we have just indicated, the tip pressure is mainly affected by the three-dimensional tip effect, rather than the rotor-wake effect, and so the underestimated effective attack-angle correction in the tip region needs to be reconsidered.

Loading Calculation with Further Angle Correction

To give a proper correction of the angle of attack in the tip region, an empirical formula for effective angle of attack can simply be constructed as follows:

$$\alpha(r) = \alpha_{\text{eff}}(r) + \beta\left(\frac{r - r_{\text{root}}}{r_{\text{tip}} - r_{\text{root}}}\right)^n [\theta_c - \alpha_{\text{eff}}(r_{\text{tip}})] \tag{7}$$

where β, n are two free parameters to be determined empirically. According to Eq. (7), the modified effective angle will take the value $\alpha_{\text{eff}}(r)$ in the root region and take the value about the collective pitch θ_c at the rotor tip. Based on some numerical tests using Eq. (7), we found that the computational pressure distributions are in excellent agreement with the experimental value at all

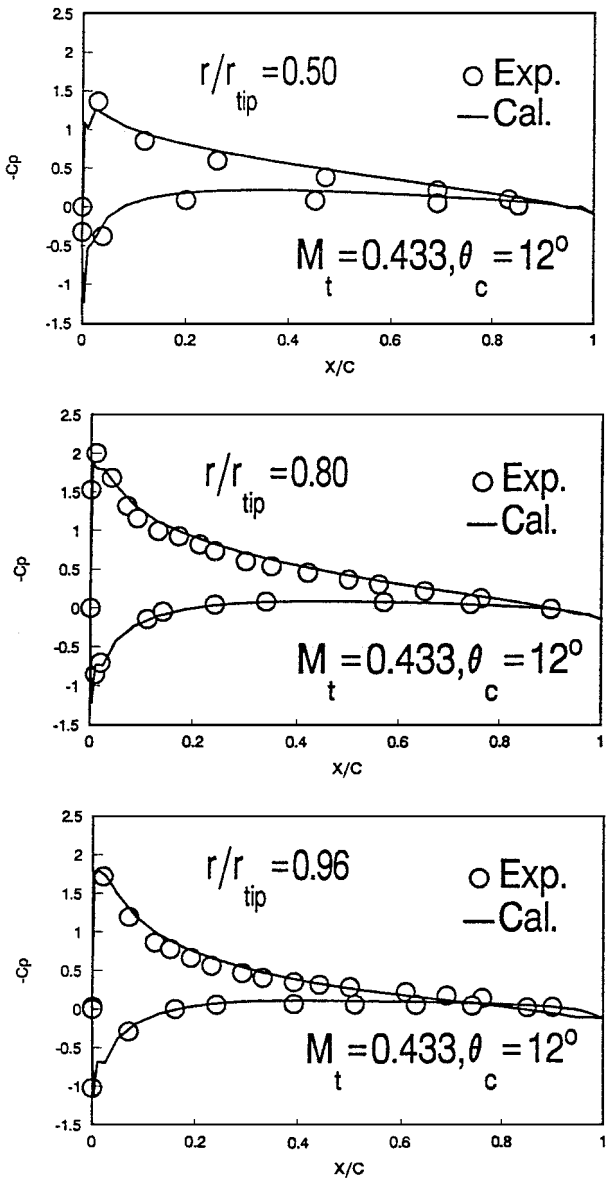

Fig. 6 Surface pressure coefficients at higher collective pitch angle.

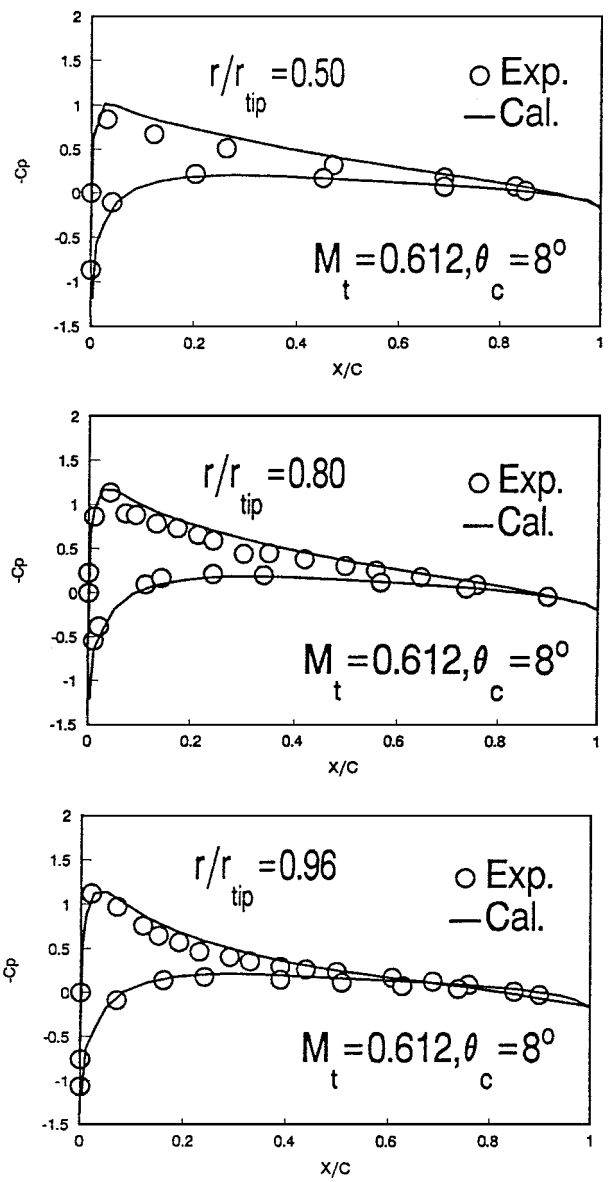

Fig. 7 Surface pressure coefficients at higher Mach number.

spanwise stations if we choose $\beta = 1.2$, $n = 3$. The corresponding distribution of the modified effective angle along the blade is shown in Fig. 5. Using the modified angle of attack, the calculated pressures are shown as Cal.(3) in Fig. 3. In this way the combined rotor-wake and blade-tip effects on the aerodynamic loading of the rotor blades are properly accounted for, although the simple expression (7) is essentially an empirical formula based on some heuristic arguments.

Further numerical calculations have been performed under the conditions listed next:

1) Increasing collective pitch angle—Figure 6 gives the pressures at the various blade spanwise stations at the higher collective pitch angle for the case $M_t = 0.433$, $Re = 2 \times 10^6$, and $\theta_c = 12$ deg. The agreement between the calculations and experiments is good. It reflects that the empirical formula for effective angle modification is proper for different blade pitch angles.

2) Increasing Mach number— Figure 7 gives the pressures at the various spanwise stations at a higher Mach number for the case $M_t = 0.612$, $Re = 2.67 \times 10^6$, and $\theta_c = 8$ deg. The agreement between the calculations and experiments is also good. The angle modification is proper for different Mach numbers.

3) Increasing Mach number and collective pitch angle—Figures 8 and 9 give the pressure comparisons between computational and experimental values for the cases $M_t = 0.520$, $Re = 2 \times 10^6$, $\theta_c = 12$ deg and $M_t = 0.610$, $Re = 2.67 \times 10^6$, $\theta_c = 12$ deg.

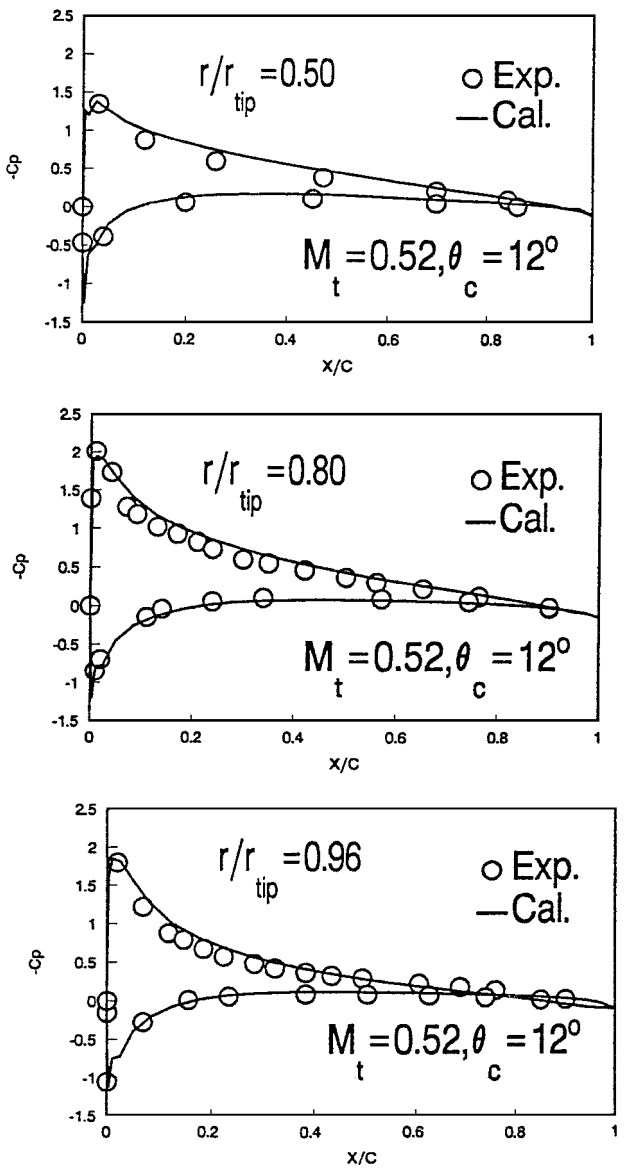

Fig. 8 Surface pressure coefficients at increased Mach number and collective pitch angle.

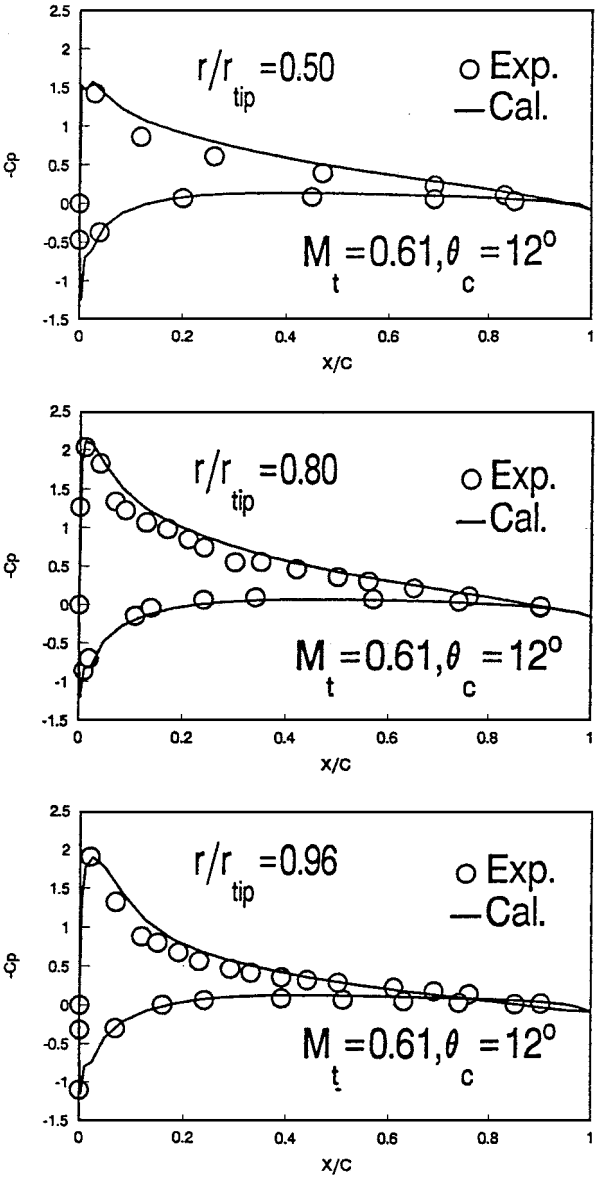

Fig. 9 Surface pressure coefficients at increased Mach number and collective pitch angle.

The agreement between the calculations and the experiments is quite satisfactory.

The empirical formula for effective angle modification is proper at least for the subsonic rotor flow.

Conclusion

In this paper an approach is presented for computing the loads of hovering helicopter rotor using the Navier–Stokes equations. To overcome the spurious numerical diffusion of vortex with coarse grid, a rotor-wake model is introduced into the computation by a modification of the local effective angle of attack along the blade, which is determined by the vortex-lattice method for potential flow in addition to an empirical correction. The validity of the present method is verified by the comparisons between the computational and experimental results.

Acknowledgment

This work is supported by the National Science Foundation in China, 19889210, and the China Research and Development Center of Aerodynamics.

References

[1]Srinivasan, G. R., Baeder, J. D., Obayashi, S., and McCroskey, W. J., "Flowfield of a Lifting Rotor in Hover: A Navier–Stokes Simulation," *AIAA Journal*, Vol. 30, No. 10, 1992, pp. 2371–2378.

[2]Berkman, M. E., and Sankar, L. N., "Navier–Stokes/Full Potential/Free-Wake Method for Rotor Flows," *Journal of Aircraft*, Vol. 34, No. 5, 1997, pp. 635–640.

[3]Roberts, T. W., and Murman, E. M., "Solution Method for a Hovering Helicopter Rotor Using the Euler Equations," AIAA Paper 85-0436, Jan. 1985.

[4]Sankar, L. N., Bharadvaj, B. K., and Tsung, F. L., "Three-Dimensional Navier–Stokes/Full Potential Coupled Analysis for Transonic Viscous Flow," *AIAA Journal*, Vol. 31, No. 10, 1993, pp. 1857–1862.

[5]Chen, C. L., and McCroskey, W. J., "Numerical Simulation of Helicopter Multi-Bladed Rotor Flow," AIAA Paper 88-0046, Jan. 1988.

[6]Bangalore, A., and Sankar, L. N., "Forward Flight Analysis of Slatted Rotors Using Navier–Stokes Methods," AIAA Paper 96-0675, Jan. 1996.

[7]Agarwal, R. K., and Deese, J. E., "Navier–Stokes Calculations of the Flowfield of a Helicopter Rotor in Hover," AIAA Paper 88-0106, Jan. 1988.

[8]Caradonna, F. X., and Tung, C., "Experimental and Analytical Studies of a Model Helicopter Rotor in Hover," NASA TM-81232, Sept. 1981.

[9]Yang, G. W., Li, J., Li, F. W., and E. Q., "Grid Generating Strategies for 3-D Realistic Aircraft Configurations," AIAA Paper 96-2461, June 1996.

[10]Jameson, A., Schmidt, W., and Turkel, E., "Numerical Solution of the Euler Equations by Finite Volume Methods Using Runge–Kutta Time-Stepping Schemes," AIAA Paper 81-1259, June 1981.

[11]Jameson, A., and Yoon, S., "Lower-Upper Implicit Schemes with Multiple Grids for the Euler Equations," *AIAA Journal*, Vol. 25, No. 7, 1987, pp. 929–935.

[12]Baldwin, B. S., and Lomax, H., "Thin Layer Approximation and Algebraic Model for Separated Turbulent Flow," AIAA Paper 78-0257, Jan. 1978.

[13]E. Q., Yang, G. W., and Li, F. W., "Numerical Analysis of the Interference Effect of Propeller Slipstream on Aircraft Flowfield," *Journal of Aircraft*, Vol. 35, No. 1, 1998, pp. 84–90.